Study on Synthesis of TPA-Silicalite-1 from Initially Clear Solutions of Various Base Concentrations by in Situ Calorimetry, Potentiometry, and SAXS

Sanyuan Yang and Alexandra Navrotsky*

Thermochemistry Facility, Department of Chemical Engineering and Materials Science, University of California at Davis, Davis, California 95616

David J. Wesolowski

Chemical and Analytical Sciences Division, Oak Ridge National Laboratory, P.O. Box 2008, Oak Ridge, Tennessee 37831-6110

John A. Pople

Stanford Synchrotron Radiation Laboratory, SLAC, P.O. Box 4349, Stanford, California 94309

Received August 4, 2003. Revised Manuscript Received October 29, 2003

The synthesis process of TPA-silicalite-1 from a series of initially clear solutions (with a general formula based on mole ratios of the components x:25:480:100 TPAOH:SiO_2:H_2O:C_2H_5OH, where TPA = tetrapropylammonium, $x = 3-13$) was investigated using small-angle X-ray scattering (SAXS), in situ calorimetry, and in situ pH measurement. The size of the nanoparticles detected in the initially clear solutions decreases from 8.5 to 2.5 nm as x increases from 3 to 13. Crystal growth from these solutions at 95 °C is first exothermic and then endothermic. The exo−endo thermal switch coincides with a jump in the solution alkalinity. With increasing x the integral heat of exothermic crystal growth decreases monotonically from −0.61 kJ/mol (per mole of Si in the mixture) at $x = 4$ and approaches zero at $x = 12$. The integral heat of endothermic crystal growth increases to approach a plateau (0.26 kJ/mol of Si) at $x = 7$. Crystal growth is fastest at $x = 6-7$ and relatively slower at x either higher than 7 or lower than 6. At $x = 6-11$ the zeolite particles assume similar spherical shape and size, about 100 nm in diameter. Outside this range ($x < 6$ or $x > 11$), particle size increases significantly. The percentage yield of the zeolite product (on silica basis) can be linearly correlated to x (yield % = 119.7 − 6.34x) from $x = 5$ to $x = 11.5$. Outside this linear zone the yield is below this trend at both lower and higher x. The thermodynamic and kinetic aspects of the synthesis process are analyzed and discussed in terms of total surface area reduction of silicate species during crystal growth, effect of surface charge density on kinetics and mechanism of crystal growth, relationship between thermal switch and solution pH jump, and the change in enthalpy and entropy of the synthesis system.

Introduction

Synthesis of zeolitic nanoparticles from initially clear solution has recently received much attention. Colloidal zeolite particles are technologically important materials because of their large external surface and favorable accessibility of their internal surfaces as adsorbent and catalyst materials. Several zeolites have been prepared as nanoparticles including Si-MFI (or silicalite-1),[1−7] Si-MTW,[5] Si-BEA,[5] Si-MEL,[7,8] LTA,[9] and FAU.[10−13] Among them, silicalite-1 is probably the most intensively studied. The initially clear solution for synthesis of silicalite-1 is usually prepared by hydrolysis of TEOS in aqueous tetrapropylammonium hydroxide (TPAOH) solution.[1,14] The so-called initially clear solutions are actually not true solutions because most of the silica is

(1) Schoeman, B. J. *Zeolites* **1997**, *18*, 97.
(2) Twomey, T. A. M.; Mackay, M.; Kuipers, H. P. C. E.; Thompson, R. W. *Zeolites* **1994**, *14*, 162.
(3) De Moor, P.-P. E. A.; Beelen, T. P. M.; Komanschek, B. U.; Beck, L. W.; Wagner, P.; Davis, M. E.; Van Santen, R. A. *Chem.−Eur. J.* **1999**, *5*, 2083.
(4) Kirschhock, C. E. A.; Ravishankar, R.; Jacobs, P. A.; Martens, J. A. *J. Phys. Chem. B* **1999**, *103*, 11021.
(5) de Moor, P.-P. E. A.; Beelen, T. P. M.; vanSanten, R. A.; Tsuji, K.; Davis, M. E. *Chem. Mater.* **1999**, *11*, 36.
(6) Nikolakis, V.; Kokkoli, E.; Tirrell, M.; Tsapatsis, M.; Vlachos, D. G. *Chem. Mater.* **2000**, *12*, 845.
(7) Testa, F.; Szostak, R.; Chiappetta, R.; Aiello, R.; Fonseca, A.; Nagy, J. B. *Zeolites* **1997**, *18*, 106.
(8) Mintova, S.; Petkov, N.; Karaghiosoff, K.; Bein, T. *Mater. Sci. Eng.* **2002**, *C19*, 111.
(9) Mintova, S.; Olson, N. H.; Valtchev, V.; Bein, T. *Science* **1999**, *283*, 958.
(10) Li, Q.; Creaser, D.; Sterte, J. *Chem. Mater.* **2002**, *14*, 1319.
(11) Mintova, S.; Valtchev, V. *Stud. Surf. Sci. Catal.* **1999**, *125*, 141.
(12) Shen, Y.; Manning, M. P.; Warzywoda, J.; Sacco, A. J. *Mater. Res. Soc. Symp. Proc.* **2002**, *740*, 241.
(13) Li, Q.; Creaser, D.; Sterte, J. *Stud. Surf. Sci. Catal.* **2001**, *135*, 151.
(14) Yang, S.; Navrotsky, A. *Chem. Mater.* **2002**, *14*, 2803.

10.1021/cm030587r CCC: $27.50
Published on Web 12/19/2003

Table 1. Syntheses of Pure Silica TPA-MFI at 95 °C from Various Initially Clear Solutions (x:25:480:100 TPAOH:SiO_2:H_2O:C_2H_5OH)

x	aging[a] (h)	crystallization (h)	synthesis mixture after crystallization[b]	solid product[c] (mg)
3	51	64	very sticky precipitate with partially clear upper liquid	406.6
4	140	41	solid suspension with no supernatant liquid	687.0
5	50	45	solid suspension with no supernatant liquid	733.1
6	90	39	solid suspension with no supernatant liquid	677.6
7	49	48	free-flow precipitate and supernatant liquid	631.5
8	12	42	free-flow precipitate and supernatant liquid	566.7
9	8	40	free-flow precipitate and supernatant liquid	518.1
10	5	43	free-flow precipitate and supernatant liquid	451.7
11	6	45	free-flow precipitate and supernatant liquid	390.6
11.5	6	41	free-flow precipitate and supernatant liquid	351.7
12	7	65	free-flow precipitate and supernatant liquid	279.8
13	6	115	sticky precipitate and supernatant liquid	91.8

[a] Time between initial mixing at room temperature and start of crystallization at 95 °C. [b] Visual appearance after in situ calorimetric synthesis. [c] All of the synthesis products are pure silica TPA-MFI by XRD and SEM (see text) and weight of air-dried solid product is from 7.5 g of initially clear solution.

already in the form of nanoparticles (composed of SiO_2, H_2O, TPA^+, and OH^- species), about 3 nm in diameter, based on small-angle X-ray/neutron scattering (SAXS/SANS).[3,15] These nanometer-sized precursor particles, referred to as primary particles, have composition and structure similar to silicalite-1 crystals.[3,16−19]

Many studies have been devoted to the understanding of the formation process of primary particles at low temperatures and their subsequent evolution to silicalite-1 crystals at elevated temperatures. Kirschhock et al.,[17] using ^{29}Si NMR, recently identified several intermediate silicate oligomers involved in the hydrolysis of TEOS in TPAOH solutions at low temperatures and illustrated a TPA-directed silicon polymerization process leading to the formation of silicalite-1 precursors.[20] Aggregation of these precursor particles to form silicalite-1 was investigated using dynamic light scattering,[1,2,6] TEM,[3,17,21] and X-ray/neutron scattering.[3,5,15,22] Previous experimental evidence is generally consistent with a crystallization mechanism of orderly aggregation of the primary particles.[3,4,6,19,20]

In this work we studied the synthesis of silicalite-1 from a series of initially clear solutions with systematic variation of the concentration of TPAOH over a much wider range than previously used in our earlier study[14] and others.[3,22,23] A combination of experimental techniques was employed in our investigation, including SAXS to characterize the primary particles in the initially clear solutions, in situ calorimetry to follow the process of crystal growth in terms of thermodynamic and kinetic description of the reaction, in situ potentiometric measurements and ex situ pH measurement to track the solution alkalinity, and scanning microscopy (SEM) and powder X-ray diffraction (XRD) to characterize the crystallized TPA-silicate-1. Our objective is to correlate various experimental observations (including size of the primary particles in the initial solutions, kinetic features of crystal growth, enthalpy/entropy change and solution pH variation during synthesis, and yield and shape/size of final zeolite crystals) with the concentration of TPAOH and to rationalize the data from viewpoints of both thermodynamics and kinetics of the synthesis events. This study is an extension of our recent endeavor using in situ calorimetry to gain a fundamental understanding of the zeolite synthesis process.[14,24−26]

Experimental Section

Preparation of Initially Clear Solutions. Solutions with compositions x:25:480:100 TPAOH:SiO_2:H_2O:C_2H_5OH, where x ranges from 3 to 13 and the coefficients reflect the relative mole ratios of the components, were prepared using tetrapropylammonium hydroxide solution (TPAOH: Alfa, 40%), tetraethyl orthosilicate (TEOS: Alfa, 99.9%), and deionized (DI) water. The preparation procedure is similar to that used in our previous report.[14] All chemical agents were used as received. The TEOS phase and the aqueous TPAOH solution were initially not miscible, forming an emulsion-like mixture under stirring. After several hours of vigorous stirring at room temperature, all of the mixtures became homogeneous and completely clear solutions to the naked eye. Aging time was taken as the period from initial mixing (of TPAOH, TEOS, and DI water) to the start of crystallization at 95 °C (Table 1).

In Situ Synthesis and Calorimetric Measurement. A Calvet-type heat flow microcalorimeter (Setaram C80) was used for in situ synthesis and calorimetric measurement. The calorimeter was operated isothermally at 95.00 ± 0.01 °C. And 7.50 g of an initial synthesis solution contained in a Teflon-lined stainless steel vessel was used. An equal mass of water was used in the reference chamber because its heat content is close to that of the synthesis system. The time of loading the sample vessel into the calorimeter at 95 °C was taken as zero crystallization time (Table 1). After the calorimeter re-established its baseline (about 3 h), the heat flow curve arising from the in situ synthesis was recorded. The energy equivalent of the calorimetric signal was calibrated electrically and

(15) Watson, J. N.; Iton, L. E.; Keir, R. I.; Thomas, J. C.; Dowling, T. L.; White, J. W. *J. Phys. Chem. B* **1997**, *101*, 10094.
(16) Schoeman, B. J.; Regev, O. *Zeolites* **1996**, *17*, 447.
(17) Kirschhock, C. E. A.; Ravishankar, R.; Verspeurt, F.; Grobet, P. J.; Jacobs, P. A.; Martens, J. A. *J. Phys. Chem. B* **1999**, *103*, 4965.
(18) Ravishankar, R.; Kirschhock, C. E. A.; Knops-Gerrits, P.-P.; Feijen, E. J. P.; Grobet, P. J.; Vanoppen, P.; De Schryver, F. C.; Miehe, G.; Fuess, H.; Schoeman, B. J.; Jacobs, P. A.; Martens, J. A. *J. Phys. Chem. B* **1999**, *103*, 4960.
(19) Kirschhock, C. E. A.; Buschmann, V.; Kremer, S.; Ravishankar, R.; Houssin, C. J. Y.; Mojet, B. L.; van Santen, R. A.; Grobet, P. J.; Jacobs, P. A.; Martens, J. A. *Angew. Chem., Int. Ed.* **2001**, *40*, 2637.
(20) Kirschhock, C. E. A.; Kremer, S. P. B.; Grobet, P. J.; Jacobs, P. A.; Martens, J. A. *J. Phys. Chem. B* **2002**, *106*, 4897.
(21) Ravishankar, R.; Kirschhock, C.; Schoeman, B. J.; Vanoppen, P.; Grobet, P. J.; Storck, S.; Maier, W. F.; Martens, J. A.; De Schryver, F. C.; Jacobs, P. A. *J. Phys. Chem. B* **1998**, *102*, 2633.
(22) De Moor, P.-P. E. A.; Beelen, T. P. M.; Van Santen, R. A. *J. Phys. Chem. B* **1999**, *103*, 1639.
(23) Persson, A. E.; Schoeman, B. J.; Sterte, J.; Otterstedt, J.-E. *Zeolites* **1994**, *14*, 557.
(24) Yang, S.; Navrotsky, A. *Microporous Mesoporous Mater.* **2002**, *52*, 93.
(25) Yang, S.; Navrotsky, A.; Phillips, B. L. *J. Phys. Chem. B* **2000**, *104*, 6071.
(26) Yang, S.; Navrotsky, A.; Phillips, B. L. *Microporous Mesoporous Mater.* **2001**, *46*, 137.

checked by using the melting enthalpies of indium and naphthalene.[24,26] As noted previously,[14] the calorimeter chamber is essentially at constant volume. Moreover, below the boiling point of the solution there is little, if any, change in pressure during synthesis. In this paper, we use the terms "enthalpy", "energy", and "energetics" essentially interchangeably because the difference between ΔE and ΔH is negligible.

After crystallization at 95 °C, the solid products were recovered by centrifugation (Beckman L8-80 M Ultracentrifuge with a 70-Ti rotor) at a relative centrifugal force of 66000 g. After centrifugation, most of the upper clear liquid was carefully removed to avoid losing any solid powder. The solid particles were re-dispersed in DI water and centrifuged again. The washing and centrifugation procedure was typically repeated four times. The solid products were dried in air (calorimeter lab area: 25 ± 1 °C and 50 ± 3% relative humidity) for at least 7 days.

Small-Angle X-ray Scattering (SAXS). The SAXS experiments were performed at Station BL1-4 at the Stanford Synchrotron Radiation Laboratory. A monochromatic X-ray beam (wavelength 0.1488 nm, beam size 500 μm (horizontal) and 250 μm (vertical) was scattered from the sample and collected on two-dimensional image plates with a 1600 × 1600 array of 50-μm square pixels with exposure times varying from 2 to 30 min. The sample-to-detector distance was 390 mm. Teflon cells with Kapton film as windows were used to hold the liquid samples. The scattering intensity, $I(q)$ (where q denotes the scattering vector, $q = (4\pi/\lambda)\sin(\theta)$, where λ and 2θ are the wavelength and the scattering angle respectively), was corrected for dark current noise in the detector, absorption from the sample, and scattering from the cell windows. The data with q from 0.1 to 3.4 nm^{-1} were radially averaged to minimize statistical fluctuations.

pH Measurements. In situ potentiometric pH measurements of the synthesis solution during the course of reaction at 95 °C were performed in a stirred hydrogen electrode concentration cell at Oak Ridge National Laboratory. The principal advantage of this cell is that we can conduct potentiometric measurements with excellent precision and accuracy at high temperature (up to 300 °C) in a highly alkaline mixture where pH measurements by conventional glass electrodes are not possible. The hydrogen electrode concentration cell design and function have been described elsewhere.[27]

In addition to in situ potentiometric measurement in the hydrogen electrode concentration cell, the 25 °C quench-pH of the synthesis solution before and after in situ calorimetric measurements was also measured using an Ag/AgCl Sure-Flow Electrode (Thermo Orion, Model 91-72BN). The electrode was calibrated using two standard buffer solutions (pH = 7.0 and 10.0) prior to each use.

Other Characterization Techniques. The crystal structure of the solid products was verified by powder X-ray diffraction (XRD) recorded on an Inel XRG 3000 diffractometer (Ni-filtered Cu Kα radiation, 30 kV, 30 mA). The resolution of the position-sensitive detector is 0.029° 2θ. The morphology of zeolite particles was examined using high-resolution scanning electron microscopy (FEI XL30 SFEG). The silica content of the solid products was determined by thermogravimetric analysis (TGA-DSC, Netzsch STA 449 C Jupiter).

Results

Synthesis and Characterization of the Solid Products. In this study, we adjusted the TPAOH concentration to prepare 12 initial synthesis mixtures, x:25:480:100 TPAOH:SiO_2:H_2O:C_2H_5OH, with x ranging from 3 to 13 (Table 1). After being stirred and aged at room temperature, all of the mixtures appeared as clear solutions, indicating the complete hydrolysis of TEOS.

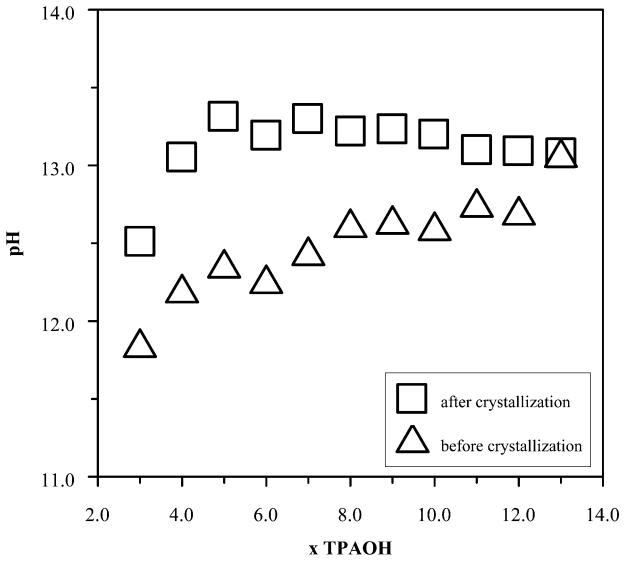

Figure 1. Solution pH measured at room temperature using glass electrode before and after crystallization of silicalite-1 at 95 °C from initially clear solutions of x:25:480:100 TPAOH:SiO_2:H_2O:C_2H_5OH.

After crystallization, however, the synthesis mixtures were visually different. At $x = 7-13$, the solid precipitate and the upper clear solution (slightly yellow colored) were well-separated. The volume of the solid precipitate decreased with increasing x from 7 to 13. At $x = 7-12$, the precipitate was easily suspended in the mother liquor by agitation. At $x = 4-6$, there was little supernatant and the final synthesis mixture remained a suspension. At $x = 3$, the synthesis mixture after crystallization consisted of an upper liquid and a lower precipitate layer. The appearance of the final synthesis mixture may be a result of several factors. Surface charging of zeolite particles in mother liquors of high pH (Figure 1) renders the product particles repulsive to one another and they are dispersed. Large particles may tend to precipitate because of the diminishing surface-charging effect relative to the gravitational effect (note that the solid density of TPA-silicalite-1 is greater than that of the liquid,[28] and Figure 2 shows particle size at different x). High x means more counterions (TPA^+) in the system (the surface of solid particles is negatively charged in high pH solution), which favors precipitation of the solid particles analogous to the de-stabilization of colloidal system by addition of salt (i.e., "salting out" effect).[29]

Solid products obtained from all of the synthesis mixtures are pure silica TPA-MFI (TPA-silicalite-1) based on their powder XRD patterns, which do not show peaks other than those of TPA-silicalite-1 or baseline humps from an amorphous component (Figure 3). SEM photos exhibit particles with well-defined shapes and no intergranular amorphous matrix (Figure 2). The crystal particles synthesized from $x = 6-11$ have the similar spheroidal shape and size (about 100 nm in diameter). Either increase of x from 11 to 13 or decrease of x from 6 to 3 leads to significant increase of particle

(27) Palmer, D. A.; Wesolowski, D. J. *Geochim. Cosmochim. Acta* **1993**, *57*, 2929.

(28) Meier, W. M.; Olson, D. H.; Baerlocher, C. *Zeolites* **1996**, *17*, 1.

(29) Maurer, T.; Kraushaar-Czarnetzki, B. *Helv. Chim. Acta* **2001**, *84*, 2550.

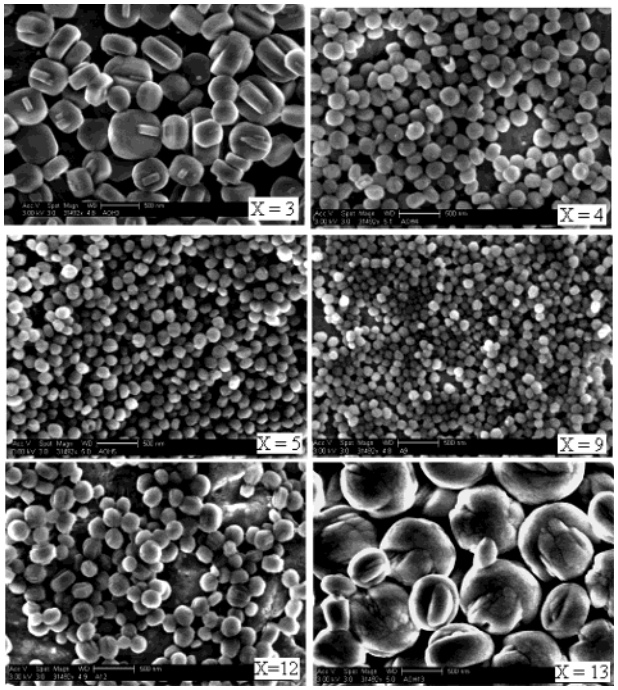

Figure 2. SEM photos of TPA-silicalite-1 synthesized at 95 °C from initially clear solutions of *x*:25:480:100 TPAOH:SiO_2:H_2O:C_2H_5OH. The SEM appearances of samples at $x = 6$, 7, 8, 10, 11, 11.5 are not shown but they are the same as that at $x = 9$. The scale bar stands for 500 nm.

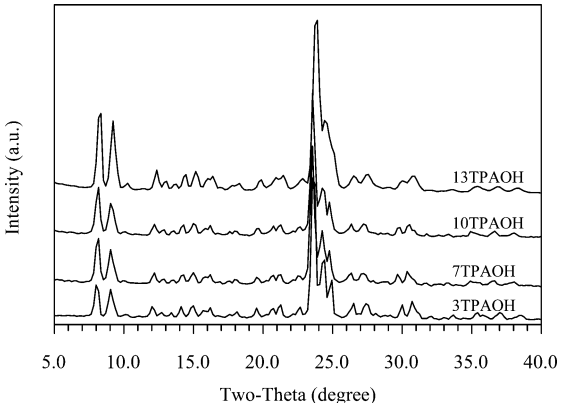

Figure 3. XRD patterns of the solid products synthesized at 95 °C from initially clear solutions of *x*:25:480:100 TPAOH:SiO_2:H_2O:C_2H_5OH.

size. Well-developed crystal edges and flat surfaces are seen for zeolite products prepared at $x = 3$, 4, 12.

The mass of the TPA-MFI product synthesized from 7.5 g of initially clear solution is listed in Table 1. The yields based on silica at different *x* are plotted in Figure 4. At $x = 5-11$, the yield drops linearly with increase of *x*. Either increase or decrease of *x* outside this linear zone produces yields significantly below the linear trend. The accelerated drop in silica yield with increase of *x* can be explained by the increase of silica solubility in basic solution. However, the drop with decrease of *x* from 5 to 3 is rather unusual. It is possible that at $x <$ 5 an increasing amount of silica nanoparticles (particle size < ca. 20 nm) remain in the reaction mixture and cannot be recovered from the synthesis solution by centrifugation.

SAXS of the Initially Clear Solutions. Particles at nanometer dimension dispersed in a matrix with

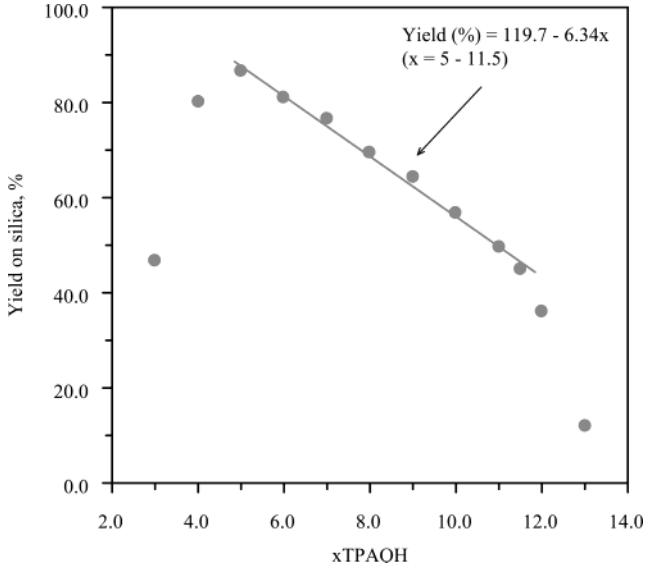

Figure 4. Yield of TPA-MFI crystals synthesized at 95 °C as a function of TPAOH usage in the initially clear solutions of *x*:25:480:100 TPAOH:SiO_2:H_2O:C_2H_5OH.

constant electronic density scatter X-rays at small angles.[30] In an isotropic medium, the SAXS intensity is a function of the modulus of the scattering vector *q*. A reciprocal law relating *q* and the length scale *d* in which a particle is being probed can be expressed as

$$d = 2\pi/q_{max} \quad (1)$$

Figure 5 shows SAXS spectra of the initially clear solutions at six selected *x* values. All spectra exhibit a single peak with a maximum located at increasing *q* values with decrease of *x*. This peak is attributed to an interference effect in X-ray scattering amplitude caused by the presence of nanometer-sized particles in the solution. The average and most probable size (*d*) of these colloidal particles can be estimated using eq 1.

Clearly, the size of the nanoparticles present in the initially clear solutions increases with decreasing *x* (Figure 6). In addition, the relative intensity of the SAXS signal increases rapidly with decreasing *x*, indicating a dramatic buildup in the population of the nanoparticles as well. SAXS of three solvent solutions *x*:480:100 TPAOH:H_2O:C_2H_5OH were also collected (Figure 5). The SAXS contribution from the solvent solutions are trivial relative to the initial synthesis clear solutions.

Thermochemistry of Crystallization at 95 °C. Heat flow curves of crystallization at different *x* values are presented in Figure 7. At $x = 3$, a very broad exothermic peak and no endothermic peak are seen. At $x = 12$, a very broad endothermic and no exothermic peak are detected. At $x = 13$, no thermal peak at all can be discerned from the baseline. Crystallization at *x* from 4 to 11.5 exhibits an exothermic peak followed by an endothermic peak. On the basis of our previous in situ calorimetric study of the same type of crystallization (from initially clear solution at $x = 9$), the heat flow curves can be interpreted as follows: (i) the onset of the exothermic peak indicates the start of self-assembly of

(30) Glatter, O.; Kratky, O. *Small Angle Scattering*; Academic Press: London, 1982.

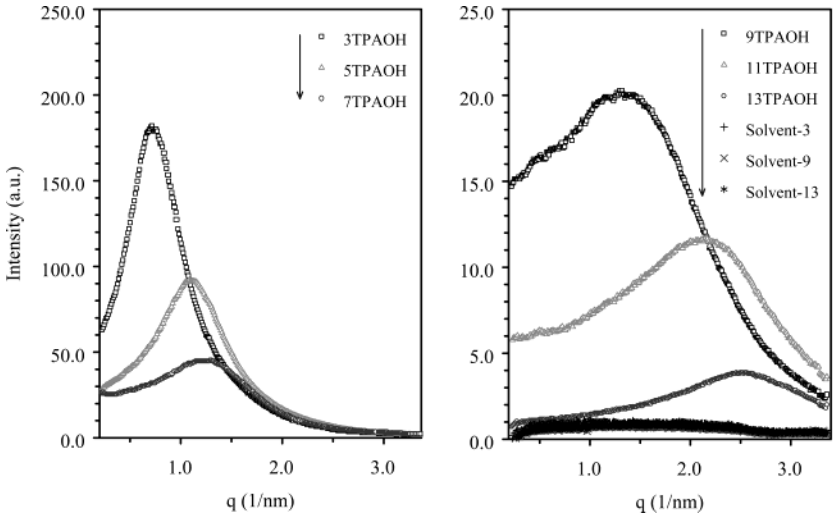

Figure 5. SAXS curves of the selected initially clear solutions of *x*:25:480:100 TPAOH:SiO_2:H_2O:C_2H_5OH prior to heating for crystallization of silicalite. Solvent-*x* has the same composition as that of initially clear solution at *x* but the SiO_2 component.

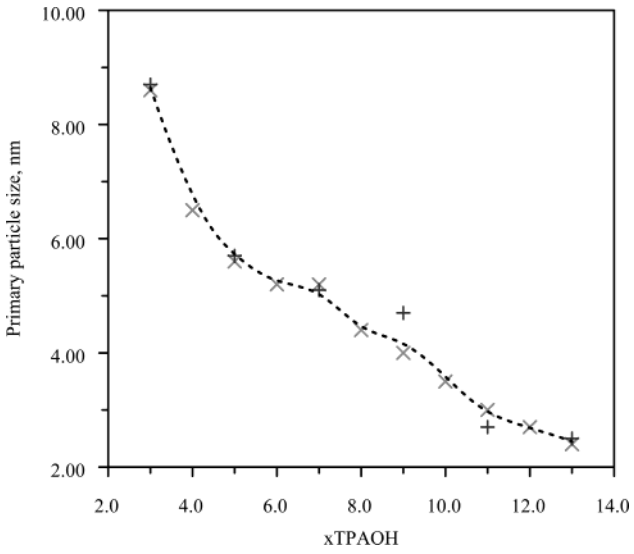

Figure 6. Average size of the primary particles present in the initially clear solutions of *x*:25:480:100 TPAOH:SiO_2:H_2O:C_2H_5OH. Two sets of symbols represent results from repeated SAXS experiments using newly prepared initially clear solutions.

the primary particles into macrocrystals; (ii) the end of the endothermic peak signals the completion of the crystallization; and (iii) the rapid exo−endo switch arises from a change in crystal growth mechanism, which leads to a jump in the solution pH (confirmed by ex situ and in situ potentiometric measurements, see additional results below).

Integral enthalpies of the exothermic peaks (ΔH_{exo}) and endothermic peaks (ΔH_{endo}) at $x = 4-12$ are plotted in Figure 8. The magnitude of ΔH_{exo} decreases monotonically from −0.61 kJ/mol (mole is based on Si in the mixture) at $x = 4$ and approaches zero at $x = 12$. Meanwhile, ΔH_{endo} increases from $x = 4$ to $x = 7$ and thereafter levels off at 0.26 kJ/mol of Si at $x = 7$. The trends of ΔH_{exo} and ΔH_{exo} in Figure 8 illustrate that, with increasing the initial TPAOH concentration, the synthesis system releases a diminishing amount of energy in the exothermic crystal growth period while it adsorbs an increasing amount of energy until a saturation level is reached at $x = 7$ in the endothermic period. Results for crystallization at $x = 3$, 12, and 13 may follow the same trend but quantitative data cannot be obtained from hump-type peaks (Figure 7).

The exo−endo peak profile describing the crystallization process shifts at different *x* values (Figure 7). Either lower than $x = 6$ or higher than $x = 7$, increasingly longer time is required for the macrocrystallization to start and complete. The reciprocal of the exo−endo thermal switch time determined from the in situ calorimetric curves (in Figure 7) may be used as an estimate of the crystal growth rate (Figure 9). There appears to be an optimum initial concentration of TPAOH at $x = 6-7$ for which the kinetics of crystallization is most favorable (see discussion below).

Monitoring Solution Alkalinity during Crystallization. To measure the pH of the synthesis solution, we used a TPAOH solution (0.0483 *m*) containing 30% EtOH as the reference solution in the hydrogen electrode concentration cell. EtOH was added in the reference solution because the synthesis solutions contain the same amount of EtOH (as a byproduct of hydrolysis of TEOS). The pH of this solution is comparable to the pH of the initial synthesis solution with $x = 9$ at room temperature. The purpose of this arrangement is to minimize the liquid junction potential and difference in H^+ activity coefficients between the sample side and the reference side. The emf response of the hydrogen electrode concentration cell was calibrated using a series of TPAOH−EtOH solutions (all contain 30% EtOH). The data were fitted by a polynomial equation and the results are presented in Figure 10. Note that the emf response of the synthesis reaction at 95 °C is limited to the low emf range (<22 mV) where the calibration curve is essentially linear. The excellent linear fitting indicates a well-behaved emf response to the change in TPAOH molal. No attempt was made to describe the speciation of these highly concentrated and complex solutions in terms of free ions and ion pairs. The results are expressed in terms of the stoichiometric TPAOH concentration of the experimental solutions relative to that of the reference solution, using the calibration curve.

The evolution of TPAOH molal in the synthesis solution during the course of reaction at 95 °C is

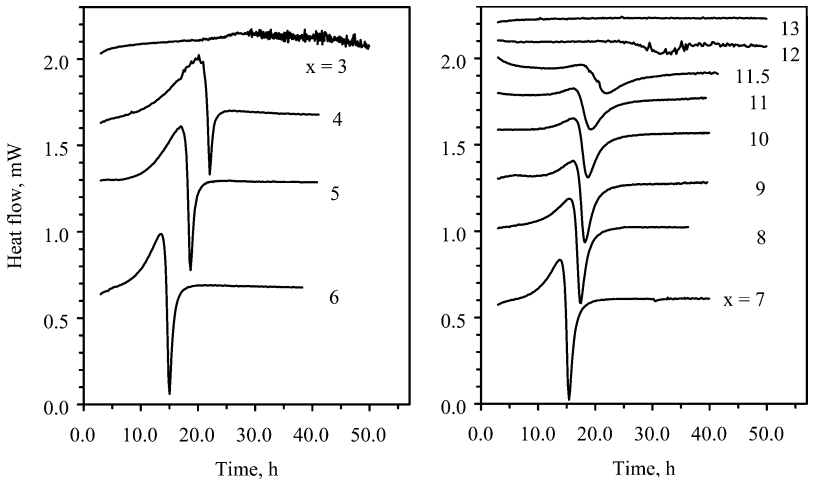

Figure 7. Heat flow curves of in situ calorimetric measurements on syntheses of silicalite-1 at 95 °C from 7.5 g of initially clear solutions *x*:25:480:100 TPAOH:SiO_2:H_2O:C_2H_5OH.

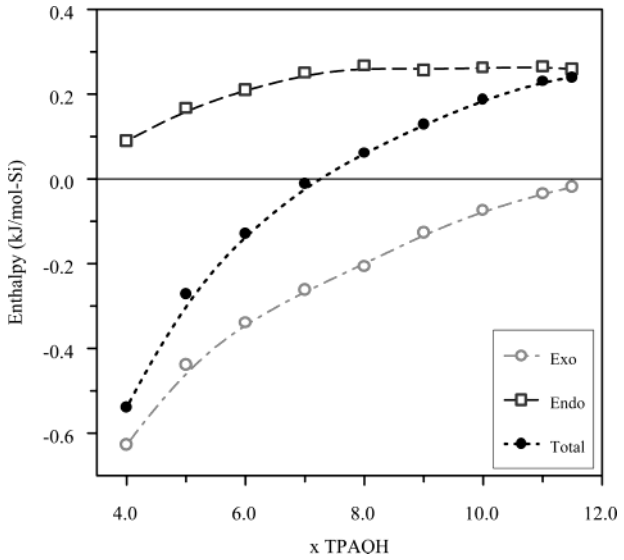

Figure 8. Integral enthalpy changes of the exothermic peak (Exo), endothermic peak (Endo), and total heat effect (Exo + Endo) from in situ calorimetric curves (in Figure 7) of crystallization of silicalite-1 at 95 °C as a function of *x* in the initially clear solutions of *x*:25:480:100 TPAOH:SiO_2:H_2O:C_2H_5OH.

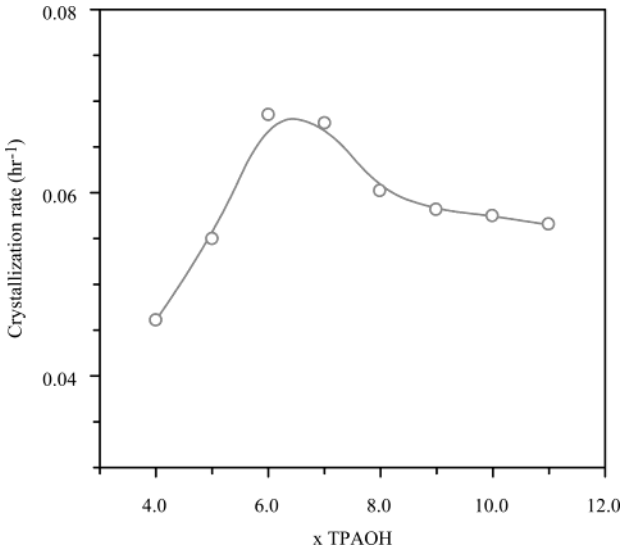

Figure 9. Reciprocal of the exo−endo thermal switch time in crystallization of silicalite-1 determined from the in situ calorimetric curves in Figure 7, an indicator of the crystallization rate, as a function of the TPAOH usage in preparation of initially clear solutions of *x*:25:480:100 TPAOH:SiO_2:H_2O:C_2H_5OH.

presented in Figure 11. The jumps in TPAOH molal at $x = 7$, 8, and 9 can be correlated with the exo−endo thermal switches in the corresponding in situ calorimetric curves (Figure 11). Quantitative correlation is not expected because in situ calorimetric experiment was conducted at static conditions and in situ potentiometric experiment requires a stirring mode. According to Kirschhock et al., stirring may slightly retard crystallization.[4] The shape of the curves shown in Figure 11 is consistent with our previous conclusion based on ex situ pH measurements: little change in the solution alkalinity before the start of endothermic crystal growth and a pH jump associated with the endothermic crystal growth. The in situ potentiometric curves exhibit additional dips near the end of the jumps. The size and shape of the dip appear to depend on *x*. At this point the exact nature of these dips is not clear.

The solution pH before and after crystallization at 95 °C was measured by a glass electrode (Figure 1). A noticeable increase in solution pH is seen after crystallization at all *x* but $x = 13$. The solution pH before crystallization increases slightly, even though *x* increases more than 4 times from 3 to 13. Likewise, the final solution pH changes little from $x = 4$ to $x = 13$. Clearly, silicate species and the charged solid surfaces impose a strong buffering effect on the solution pH.

The pH measurements suggest that the free TPAOH concentration in the synthesis solution is substantially lower than the TPAOH concentration represented by *x* in the composition formula (*x*:25:480:100 TPAOH:SiO_2:H_2O:C_2H_5OH). But *x* still reflects the general trend of the solution alkalinity because the pH of the synthesis solution is generally higher at increasing *x* before crystallization (Figure 1) and remains unchanged during exothermic crystallization (Figure 11).

Discussion

Pure silicalite-1 was synthesized from the initial solutions at *x* ranging from 3 to 13 (Table 1 and Figures 2 and 3), manifesting the robust synthesis system for MFI framework structure in the presence of TPA ions.

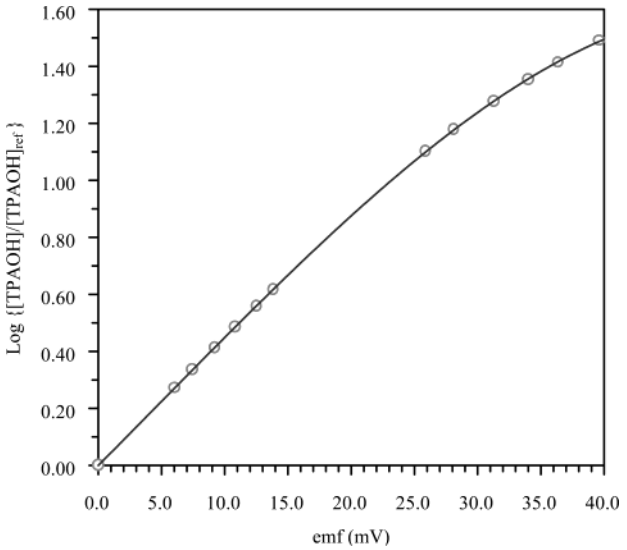

Figure 10. Calibration curve of $\log\{[TPAOH]/[TPAOH]_{ref}\}$ vs emf measured on the hydrogen electrode concentration cell. Note: $[TPAOH]_{ref} = 0.0483$ M. All experiments were done in the linear regime.

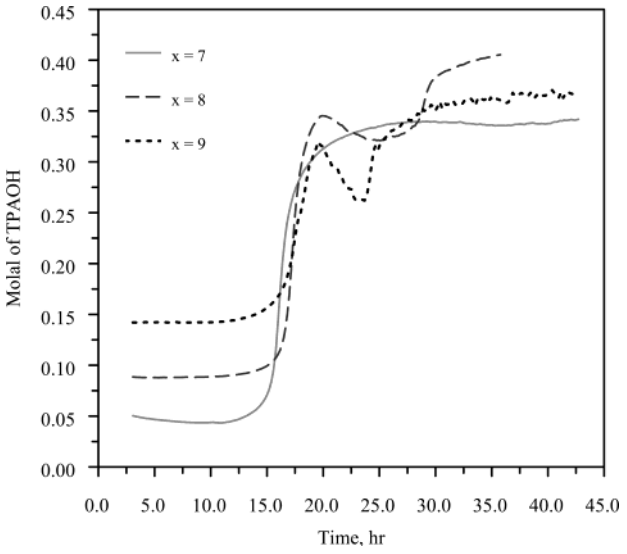

Figure 11. In situ potentiometric measurement of solution TPAOH molal during crystallization of silicalite-1 at 95 °C from initially clear solutions of *x*:25:480:100 TPAOH:SiO_2:H_2O:C_2H_5OH.

For stoichiometric conversion of all the silica in the initial solutions of *x*:25:480:100 TPAOH:SiO_2:H_2O:C_2H_5-OH to TPA-silicalite-1, the required TPA concentration as the structure-directing agent is equivalent to $x = 1$. The structure-directing agent effect of TPA ions is apparently well-saturated at $x \geq 1$; the TPAOH concentration applied in the synthesis ($x \gg 1$) primarily reflects the base concentration.

Electrophoretic measurements by Maurer et al.[31] and Schoeman and Sterte[32] showed an isoelectric point (iep) of the surface of TPA-silicalite-1 and silicalite-1 nanoparticles at pH ~ 6. Similar or lower pH_{iep} were reported for various silica glasses.[33] Our recent potentiometric titration of the TPA-silicalite-1 nanoparticles in solutions of different ionic strengths suggest a point of zero charge of the solid at pH = 7.7 (25 °C) and 7.2 (50 °C) (unpublished results). The surface charge density corresponding to pH similar to the synthesis conditions is not readily accessible by experiments because the dissolution of the zeolite increases rapidly at pH > 10. The dissolution problem becomes more significant at increasing temperature. But it is clear that the TPA-silicalite-1 particles (as well as silicate oligomers) are negatively charged in the synthesis solution (pH > 12) and the surface charge density can be expected to increase at increasing pH.

Our SAXS results show that the primary particles formed in the initially clear solutions at room temperature are smaller with use of more TPAOH (Figure 6). This may be explained from a kinetic viewpoint. Higher base concentration means higher surface charge density of the silicate oligomers (formed from early-stage hydrolysis of TEOS at room temperature[20]). Higher surface charge density increases the energy barrier for the charged silicate species to coalesce and grow to form the primary particles. At a given *x*, growth of the primary particles will consume silicate oligomers,[20] reduce the total surface area of silicate species, and consequently increase surface charge density and/or release more base to solution. The implication is that the growth of the primary particles at room temperature up to a certain size will be kinetically self-inhibited. In this way the TPAOH concentration controls the average size of the primary particles formed in the initially clear solutions. From a thermodynamic viewpoint, however, the clear solutions are metastable toward growing even larger primary particles or eventually silicalite-1 crystals, except probably at a very high TPAOH concentration (see further discussion).

Heating the initial solutions from room temperature to 95 °C has both thermodynamic and kinetic impact on crystal growth. The gain in kinetic energy of the primary particles (associating by Brownian motion) facilitates the rate of collisions, and therefore coalescence of the primary particles. The smaller the primary particles (in solutions at higher *x* values), the more relative gain in kinetic energy on a per mass basis because the kinetic energy of each primary particle (kT) is independent of particle size/mass. As a result, the smaller the primary particles, the more relative gain in the rate of crystallization at elevated temperatures. This may explain why crystallization of silicalite-1 can take place slowly even from a highly basic solution ($x = 13$) at 95 °C, in which the kinetic barrier should be quite significant as discussed earlier. Figure 9 shows that that the crystal growth proceeds increasingly more slowly from $x = 7$ to $x = 11$, indicating increasingly unfavorable kinetics. Kinetic considerations based on arguments of surface charge density and repulsion of the charged silica particles may explain the trend seen in this range of TPAOH concentration. However, the same considerations would predict a steady increase in crystallization rate from $x = 6$ to $x = 3$, which is opposite the trend observed (Figure 9).

To reconcile this contradiction and explain other experimental observations, we propose a two-step scheme for crystal growth of silicalite-1 (see schematic presentation in Figure 12) based on an orderly aggregation

(31) Maeurer, T.; Mueller, S. P.; Kraushaar-Czarnetzki, B. *Ind. Eng. Chem. Res.* **2001**, *40*, 2573.
(32) Schoeman, B. J.; Sterte, J. *Kona* **1997**, *15*, 150.
(33) Kosmulski, M. *Surf. Sci. Ser.* **2001**, *102*, 197.

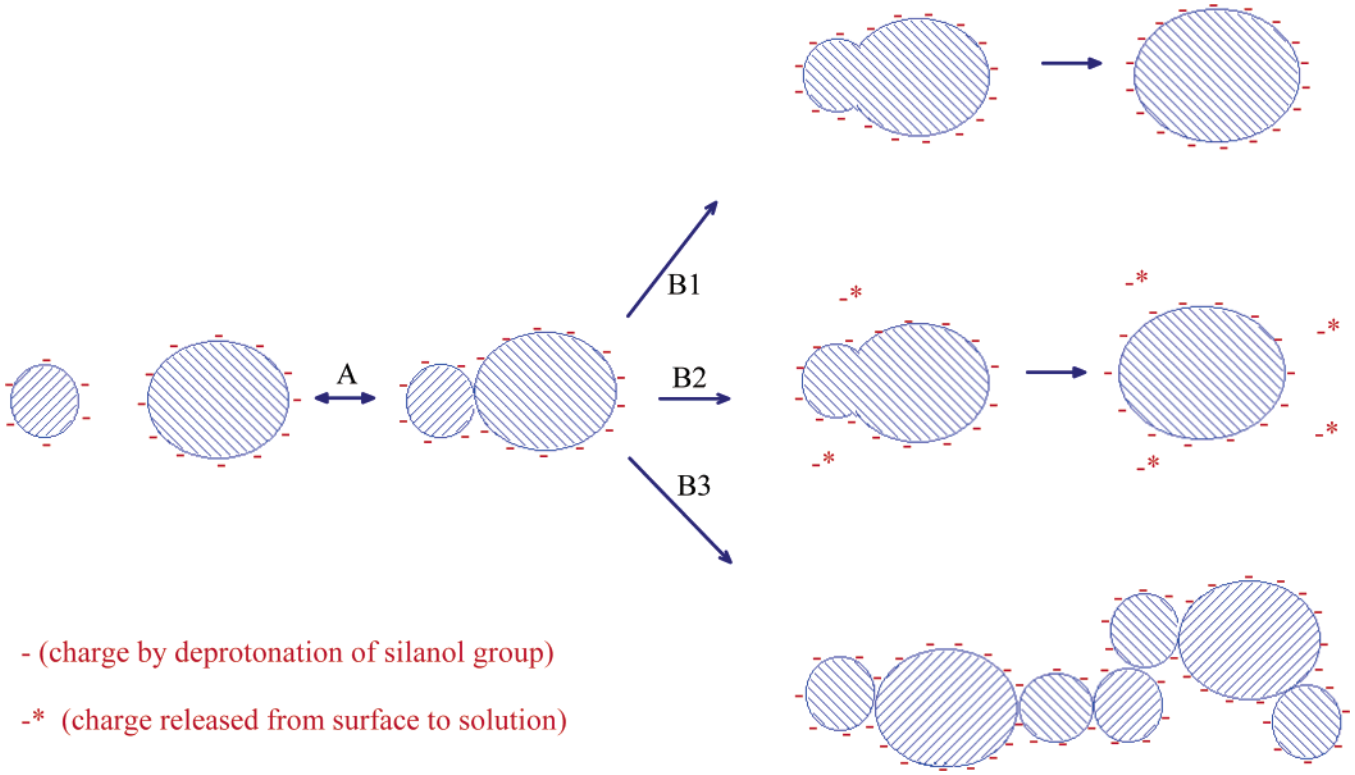

Figure 12. Schematic presentation for crystal growth of TPA-silicalite-1: step A = attachment of a PP to a growing crystal; step B1 = structural orientation alignment and mergence of the PP and growing crystal during which no net charge is released to solution; step B2 = same as B1 but some surface charge is released to solution; and step B3 = attachment continues before mergence of previously attached particles completes.

mechanism of pre-assembled primary particles.[3,6,19,20,34,35] In step one, a primary particle collides with a growing crystal and attaches to its surface (step A in Figure 12). The attachment is loose and the particles may be joined only at a few points. The combined surface area of the two particles is not significantly changed. This event only slightly affects the surface charge density. Attachment may be mostly entropy-driven because the event yields little stabilization (or even some destabilization) in energetics of the system but a gain in entropy by eliminating some surface-adsorbed molecules such as water and/or ethanol into solution. In step two, the attached primary particle aligns its orientation so that epitaxy with the growing crystal is fulfilled and the two particles merge (step B1 or B2). The total surface area of the two merging particles decreases significantly in this step. To accommodate the charges on the eliminated surface, the surface charge density of the remaining particles must either increase (step B1 in Figure 12) or the charges (or hydroxyl groups) are released into solution, causing a rise in solution pH (step B2 in Figure 12). The former route is designated as A → B1 and the latter route as A → B2. One of the two routes is likely dominant except at the transition region of the two routes.

In the attachment step, the repulsive force between the negatively charged surfaces of individual silicate species or particles creates an energy barrier. Decreasing base concentration reduces the surface charge density of silicate species and favors the kinetics of attachment. The step involving alignment/merging of particles requires breaking and reforming Si−O−Si bridges, which is catalyzed by base. Increasing base concentration should facilitate this reaction. The opposing trends of the reaction rates in these two steps as a function of base concentration (x) are presented schematically in Figure 13: with an increase of x, the rate of attachment (step A) decreases and that of alignment (steps B1 and B2) increases. As a result, the crystal growth is most favorable at medium TPAOH concentrations, which is consistent with experimental observation (Figure 9). This discussion suggests an optimum base concentration for crystal growth, not too strong to prevent attachment to occur yet sufficient for realignment to be kinetically viable. The slow rate of crystal growth usually favors the formation of large crystals consistent with the experimental observation of significant larger crystals at either low or high x (Figure 2).

At high x, a primary particle, once attached, is rapidly realigned and merged into the growing crystals. In such a scenario the growing crystals and primary particles are expected to be spatially well-separated in solution. On the other hand, at low x, prior to being fully embedded into the growing crystal structure, the randomly attached primary particles may tend to coalesce with other primary particles and/or other growing crystals (step B3 in Figure 12). At elevated temperatures and/or with time, the randomly aggregated particles can transform into an extended ordered structure of TPA-silicalite-1. This route (A → B3) may be viewed as a variant of A−B1 at very low x. Interestingly, route A → B3 may explain the observation of flocculent-like

(34) Kirschhock, C. E. A.; Ravishankar, R.; Van Looveren, L.; Jacobs, P. A.; Martens, J. A. *J. Phys. Chem. B* **1999**, *103*, 4972.
(35) Banfield, J. F.; Welch, S. A.; Zhang, H.; Ebert, T. T.; Penn, R. L. *Science* **2000**, *289*, 751.

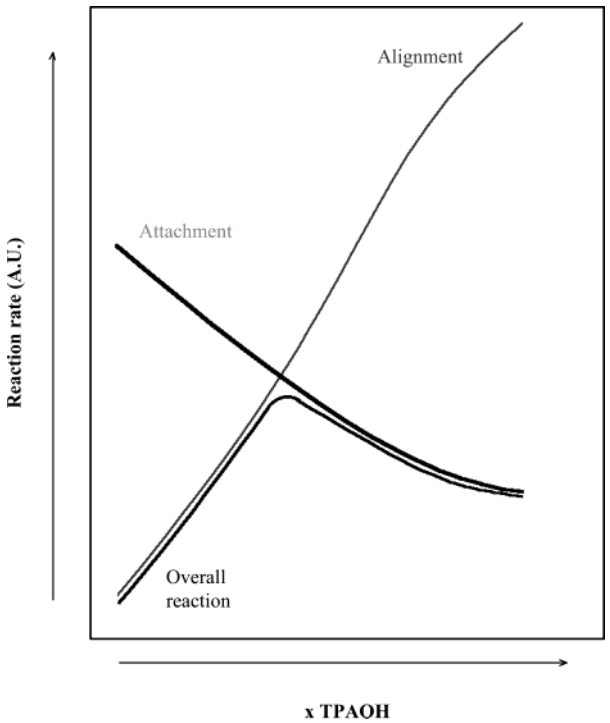

Figure 13. Schematic representation of the effect of TPAOH concentration in the initially clear solutions (x:25:480:100 TPAOH:SiO_2:H_2O:C_2H_5OH) on the reaction rate of (i) attachment of PPs onto the growing TPA-silicalite-1 crystals, (ii) alignment of the attached PPs, and (iii) overall crystal growth.

suspensions before, during, and after crystallization at low x (3−5) while also explaining the observation of a cloudy suspension only during crystal growth at high x (7−13). Consistent with this discussion, we could not prepare a clear solution at $x = 2$ (corresponding to a composition of 2:25:480:100 TPAOH:SiO_2:H_2O:C_2H_5OH) but rather we obtained a glasslike gel, indicating that a random aggregation of the primary particles with a very large porosity already occurs at room temperature. Another interesting experimental observation is the formation of a cloudy suspension from the initially clear solution at $x = 9$ upon addition of acid solution to partially neutralize the base. These observations are consistent with the reported behavior of aggregation of TPA-silicalite-1 sol at different pH.[29]

In situ calorimetric results show that the growth of silicalite-1 can proceed either with negative or with positive change in enthalpy of the total synthesis system. Endothermic heat flow or the positive change in enthalpy ($\partial H/\partial \xi \geq 0$, where ξ stands for the extent of reaction) implies the presence of positive entropy to drive the reaction forward according to the second thermodynamic law:

$$\partial G/\partial \xi = \partial H/\partial \xi - T\partial S/\partial \xi$$

The positive change in entropy is attributed to the release of water and/or hydroxide molecules from the eliminated surface of silicate species into solution during crystal growth. Unlike the energetic driving force, the entropy driving force is present throughout (both exothermic and endothermic) crystal growth and remains relatively constant.[14] An entropy-driving force means that growth of the primary particles or crystallization is thermodynamically enhanced at higher temperatures (within limits of occurrence of other competitive phases).

We have previously reported that at $x = 9$ crystal growth is first exothermic and then endothermic. The exo−endo thermal switch coincides with a pH jump in the synthesis solution. The experimental results of this study **(**Figure 6) display the same type of exo−endo switch during the period of crystal growth over a wide range of x (4−11). Furthermore, in situ potentiometric measurements (Figure 11) confirm the correlation between the exo−endo thermal switch and abrupt change in solution alkalinity. The experimental observation was previously interpreted based on a crystal growth mechanism by orderly aggregation of primary particles. It was argued that, in the exothermic stage, crystal growth and elimination of surface area cause little change in solution pH because of a surface charge density increase. When the surface charge density increase can no longer be tolerated energetically, hydroxyl is released from the surface into solution, leading to the thermal switch to endothermic crystal growth and rise in solution pH. This rationalization about the interplay among thermal switch, surface charge density, and solution chemistry remains applicable when other silica oligomers in the synthesis mixture are taken into account. One may visualize all silicate species (including soluble monomer and oligomers) as having a "surface". The total surface area always decreases as the crystal growth proceeds regardless of mechanism. A more general statement can then be made: crystal growth (in a closed system) by aggregation of the same-charge particles is always associated with an increase in average surface charge density and/or solution pH (assuming the surface is negatively charged), regardless of solution speciation and crystal growth mechanism.

The primary particles are already formed in the initial solution at room temperature and the crystal growth at 95 °C consumes the primary particles.[3,4,6] The integral heat of the exothermic peak (ΔH_{exo}) in Figure 8 gives a measure of the energetic metastability of the initial solution along the crystal growth pathway. Integral heat of the endothermic peak (ΔH_{endo}) measures how high the synthesis system can climb on an energy wall (driven by entropy force as discussed earlier). The $\Delta H_{exo} \sim x$ plot (Figure 8) implies that using higher concentration of base ($x = 4 \rightarrow 11.5$) gradually eliminates the energetic metastability from the initial synthesis solution. In situ calorimetry measures the enthalpy of the whole system, particles plus solution (gas phase has a negligible effect). Our calorimetric results show that a system containing small primary particles is energetically less stable than one with large particles at low alkalinity, but this difference becomes smaller in magnitude as alkalinity increases. At very high pH the system with smaller particles may even become energetically more stable than that with large particles. This does not necessarily imply that the small particles, by thermodynamics, are less or more stable than the large ones. Indeed such a comparison cannot be made directly since the particles are changing compositions (releasing H_2O and OH^- to solution) as they grow. So one can only discuss the energetic stability of the particles based on the direction of the energetic change in the whole system (particles plus solution).

The $\Delta H_{endo} \sim x$ plot (Figure 8) exhibits a gradual increase in the energy of the synthesis system from $x =$

4 → 7 and thereafter a plateau, indicating that at high base concentration the entropy-driving force can push the synthesis system (along the pathway of crystal growth) to a higher energy state, which is, however, limited by the magnitude of molar entropy change. The plot of ΔH ($= \Delta H_{exo} + \Delta H_{endo}$) $\sim x$ (Figure 8) demonstrates that the synthesis system after crystallization can either release or absorb net energy depending on the base concentration added in the initial solution. Note that all the observed enthalpies are small in magnitude ($\leq$0.6 kJ/mol of SiO_2). This is further confirmation that the reaction process is the assembly of pre-existing particles rather than the much more energetic process relating to polymerization and acid−base reactions. Furthermore, it is the increase of the system entropy rather than the evolution of the synthesis system energy that is always present and constantly drives the reaction forward. For this reason, temperature may not only have significant effect on the rate of crystal growth (kinetic factor) but also may slightly enhance the extent of the reaction (thermodynamic factor).

Now let us examine the thermodynamic stability of the initial solutions containing primary particles. To a first approximation, we may assume the same $\partial H/\partial \xi$ and $\partial S/\partial \xi$ for further growth of the primary particles at room temperature as for early crystal growth at 95 °C. At $x < 12$ all crystal growths are initially exothermic (Figure 7), that is, $\partial H/\partial \xi < 0$. Then $\partial G/\partial \xi$, for further growth of the primary particles at room temperature, can be assumed negative (because $\partial S/\partial \xi < 0$, see preceding discussion), suggesting that these initial solutions are thermodynamically metastable. Indeed, after a long time of aging (2 years) at room temperature, we were able to collect silicalite-1 crystals from an initially clear solution of 9:25:480:100 TPAOH:SiO_2:H_2O:C_2H_5OH (detailed study about aging effects will be reported separately). As shown in Figure 8, the thermodynamic metastability of the initially clear solution at room temperature decreases with increase of x. At $x \geq 12$, the trend of the in situ calorimetric curves (Figure 7) suggests that the onset of crystal growth at 95 °C may shift from an exothermic event to an endothermic one, implying a positive $\partial H/\partial \xi$ term. Then the $\partial S/\partial \xi$term may not be sufficient to balance the positive $\partial H/\partial \xi$ term at lower temperature so that the synthesis solution may become thermodynamically stable against further particle growth at room temperature.

In conclusion, we found that a higher TPAOH concentration favors the formation of smaller primary particles and reduces the energetic metastability of the initial solution. Crystal growth is first exothermic and then endothermic. The exo−endo switch during crystal growth is associated with an increase of the solution alkalinity. Crystal growth is fastest at medium TPAOH concentrations. These results can be explained in terms of (a) repulsion between silicate species, which is in turn influenced by the balance of surface charge density, solution hydroxyl concentration, and initial base concentration, (b) thermodynamics and kinetics of crystal growth, and (c) a two-step mechanism of crystal growth, that is, attachment of a primary particle to growing crystal followed by the alignment and merging.

Acknowledgment. We thank M. Wang (UCD) for help in SEM experiments and P. Benezeth (ORNL) for help in potentiometric measurements. We acknowledge the support of the Stanford Synchrotron Radiation Laboratory, U.S. Department of Energy, in providing the X-ray scattering facilities used in this work, supported by Department of Energy Contract DE-AC03-76SF00515. In situ pH measurements were conducted with support from the U.S. Department of Energy, Office of Basic Energy Sciences, under Contract DE-AC05-00OR22725 with Oak Ridge National Laboratory, managed and operated by UT-Battelle, LLC. This work was supported by the National Science Foundation, Grant DMR-01-01391.

CM030587R